Crystal structure of indacaterol hydrogen maleate ($C_{24}H_{29}N_2O_3$)($HC_4H_2O_4$)

James A. Kaduk,[1,2,a)] Megan M. Rost,[3] Anja Dosen,[3] and Thomas N. Blanton[3]
[1]*Illinois Institute of Technology, 3101 S. Dearborn St., Chicago, IL 60616, USA*
[2]*North Central College, 131 S. Loomis St., Naperville, IL 60540, USA*
[3]*ICDD, 12 Campus Blvd., Newtown Square, PA 19073-3273, USA*

(Received 3 December 2023; accepted 27 January 2024)

The crystal structure of indacaterol hydrogen maleate has been solved and refined using synchrotron X-ray powder diffraction data, and optimized using density functional techniques. Indacaterol hydrogen maleate crystallizes in space group *P*-1 (#24) with $a = 8.86616(9)$, $b = 9.75866(21)$, $c = 16.67848(36)$ Å, $\alpha = 102.6301(10)$, $\beta = 94.1736(6)$, $\gamma = 113.2644(2)°$, $V = 1273.095(7)$ Å^3, and $Z = 2$ at 295 K. The crystal structure consists of layers of cations and anions parallel to the *ab*-plane. Traditional N–H···O and O–H···O hydrogen bonds link the cations and anions into chains along the *a*-axis. There is a strong intramolecular charge-assisted O–H···O hydrogen bond in the non-planar hydrogen maleate anion. There are also two C–H···O hydrogen bonds between the anion and cation. The cation makes a strong N–H···O hydrogen bond to the anion, but also acts as a hydrogen bond donor to an aromatic C in another cation. The amino group makes bifurcated N–H···O hydrogen bonds, one intramolecular and the other intermolecular. The hydroxyl group acts as a donor to another cation. The powder pattern has been submitted to ICDD for inclusion in the Powder Diffraction File™ (PDF®).
© The Author(s), 2024. Published by Cambridge University Press on behalf of International Centre for Diffraction Data. This is an Open Access article, distributed under the terms of the Creative Commons Attribution licence (http://creativecommons.org/licenses/by/4.0/), which permits unrestricted re-use, distribution and reproduction, provided the original article is properly cited.
[doi:10.1017/S0885715624000071]

Key words: indacaterol, Arcapta, crystal structure, Rietveld refinement, density functional theory

I. INTRODUCTION

Indacaterol maleate (as the 1:1 salt, marketed under the trade names Arcapta and Onbrez, among others) is used for the treatment of chronic obstructive pulmonary disease (COPD) as a long acting β-adrenoceptor agonist. Indacaterol is included in the Top 200 Small Molecule Drugs by Retail Sales in 2022 (McGrath et al., 2010). The systematic name of indacaterol maleate (CAS Registry Number 753498-25-8) is 5-[(1R)-2-[(5,6-diethyl-2,3-dihydro-1H-inden-2-yl)amino]-1-hydroxyethyl]-8-hydroxy-1H-quinolin-2-one (Z)-but-2-enedioic acid. A two-dimensional molecular diagram of indacaterol maleate is shown in Figure 1.

The crystal structure of indacaterol maleate has been reported by Baur et al. (2010; Novartis; CSD Refcode YIBRAG) in space group *P*1, with $Z = 2$. There are thus two independent cations and two independent anions in the structure, but the crystal structure is not discussed in any detail. There is currently no powder pattern calculated from this structure in the Powder Diffraction File (Gates-Rector and Blanton, 2019). Both PLATON (Spek, 2009) and checkCIF (Spek, 2020) suggest the presence of a center of symmetry, and thus that the true space group is *P*-1.

This work was carried out as part of a project (Kaduk et al., 2014) to determine the crystal structures of large-volume commercial pharmaceuticals, and include high-quality powder diffraction data for them in the Powder Diffraction File.

II. EXPERIMENTAL

Indacaterol maleate was a commercial reagent, purchased from TargetMol (Batch #144181), and was used as-received. The white powder was packed into a 1.5-mm diameter Kapton capillary, and rotated during the measurement at ~50 Hz. The powder pattern was measured at 295 K at a beam line of 11-BM (Antao et al., 2008; Lee et al., 2008; Wang et al., 2008) of the Advanced Photon Source at Argonne National Laboratory using a wavelength of

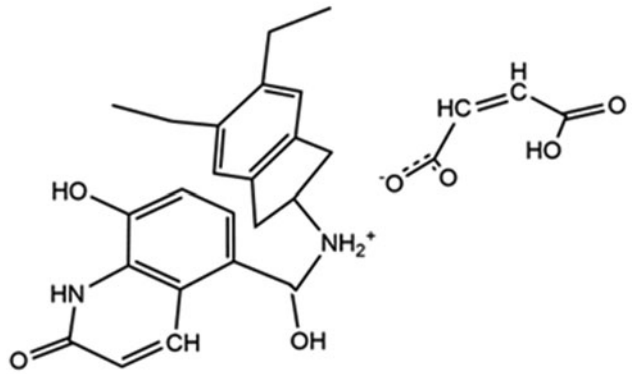

Figure 1. The two-dimensional structure of indacaterol hydrogen maleate.

a)Author to whom correspondence should be addressed. Electronic mail: kaduk@polycrystallography.com

Downloaded from https://www.cambridge.org/core. 23 Nov 2024 at 01:21:51, subject to the Cambridge Core terms of use.

0.459744(2) Å from 0.5° to 40° 2θ with a step size of 0.001° and a counting time of 0.1 s/step. The high-resolution powder diffraction data were collected using twelve silicon crystal analyzers that allow for high angular resolution, high precision, and accurate peak positions. A mixture of silicon (NIST SRM 640c) and alumina (NIST SRM 676a) standards (ratio Al_2O_3:Si = 2:1 by weight) was used to calibrate the instrument and refine the monochromatic wavelength used in the experiment.

The pattern was indexed using N-TREOR (Altomare et al., 2013) on a primitive triclinic unit cell with a = 8.86565, b = 9.76041, c = 16.67825 Å, α = 102.640, β = 94.169, γ = 113.266°, V = 1273.2 Å^3, and Z = 2. Since indacaterol is not a chiral molecule, we assumed the space group to be P-1, which was confirmed by successful solution and refinement of the structure. A reduced cell search in the Cambridge Structural Database (Groom et al., 2016) yielded three hits, including Refcode YIBRAG (Baur et al., 2010) for indacaterol maleate.

The indacaterol molecule was downloaded from PubChem (Kim et al., 2023) as Conformer3D_CID_6918554.sdf, and was converted into a .mol2 file using Mercury (Macrae et al., 2020). The structure of the hydrogen maleate anion was extracted from the crystal structure of rosiglitazone hydrogen maleate hydrate (Cuffini et al., 2008), and saved as a .mol2 file using Materials Studio (Dassault, 2022). The structure was solved by Monte Carlo-simulated annealing techniques as implemented in EXPO2014 (Altomare et al., 2013). A neutral indacaterol molecule and a hydrogen maleate anion were used as fragments. All four torsion angles in the anion were fixed, to make it a rigid body. Analysis of potential hydrogen bond interactions made it clear that N4 was protonated, and H69 was added to that atom using Materials Studio.

Rietveld refinement was carried out with GSAS-II (Toby and Von Dreele, 2013). Only the 1.5°–25.0° portion of the pattern was included in the refinements (d_{min} = 1.062 Å). All non-H bond distances and angles were subjected to restraints, based on a Mercury/Mogul Geometry Check (Bruno et al., 2004; Sykes et al., 2011). The Mogul average and standard deviation for each quantity were used as the restraint parameters. The quinoline and phenyl rings were restrained to be planar. The restraints contributed 10.1% to the final χ^2. The hydrogen atoms were included in calculated positions, which were recalculated during the refinement using Materials Studio (Dassault, 2022). The U_{iso} of the C, N, and O atoms were grouped by chemical similarity. The U_{iso} for the H atoms were fixed at 1.3× the U_{iso} of the heavy atoms to which they are attached. The peak profiles were described using a uniaxial microstrain model, with 001 as the unique axis.

The final refinement of 137 variables using 23,538 observations and ninety-five restraints yielded the residuals R_{wp} = 0.13002 and GOF = 1.62. The largest peak (0.58 Å from N4) and hole (1.684 Å from C13) in the difference Fourier map were 0.75(10) and −0.47(10) eÅ^{-3}, respectively. The final Rietveld plot is shown in Figure 2. The largest features in the normalized error plot represent subtle errors in peak positions, and probably indicate changes to the specimen during the measurement.

The crystal structure of indacaterol hydrogen maleate was optimized (fixed experimental unit cell) with density functional techniques using VASP (Kresse and Furthmüller, 1996) through the MedeA graphical interface (Materials Design, 2016). The calculation was carried out on 16 2.4-GHz processors (each with 4-Gb RAM) of a 64-processor HP Proliant DL580 Generation 7 Linux cluster at North Central College. The calculation used the GGA-PBE functional, a plane wave cutoff energy of 400.0 eV, and a k-point spacing of 0.5 Å^{-1} leading to a 2 × 2 × 1 mesh, and took ~9.9 h. Single-point density functional calculations (fixed experimental cell) and population analysis were carried out using CRYSTAL23 (Erba et al., 2023). The basis sets for

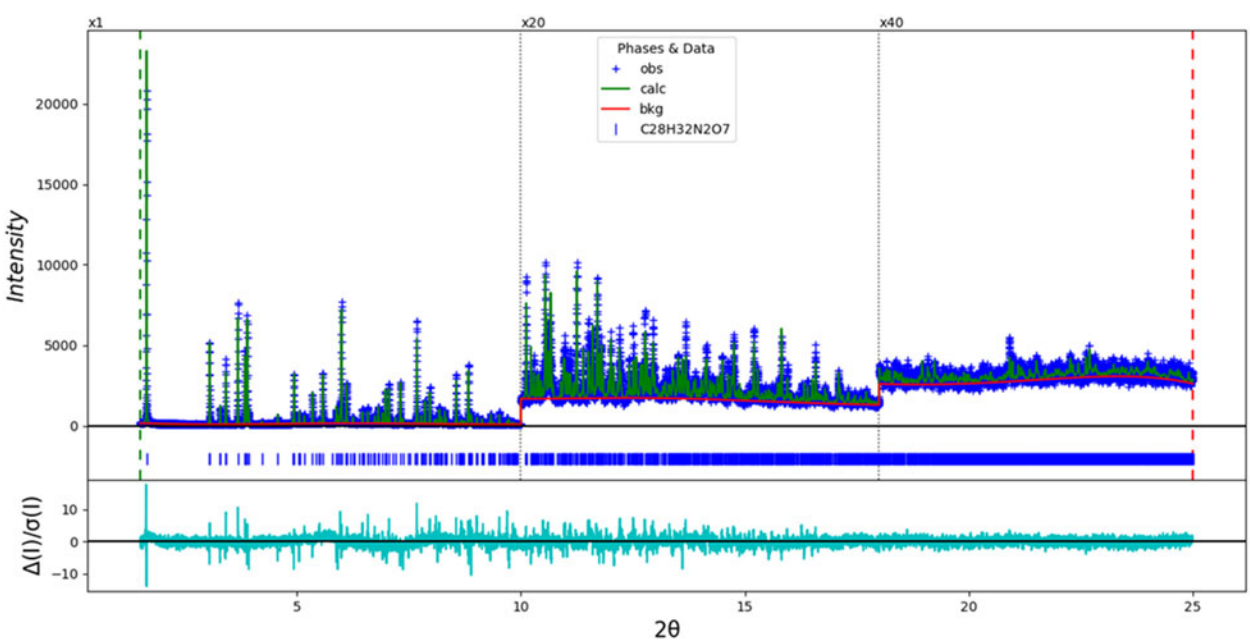

Figure 2. The Rietveld plot for the refinement of indacaterol hydrogen maleate. The x-axis is 2θ, and the y-axis is counts. The blue crosses represent the observed data points and the green line is the calculated pattern. The cyan curve is the normalized error plot and the red line is the background curve. The vertical scale has been multiplied by a factor of 20× for 2θ > 10.0° and by a factor of 40× for 2θ > 18.0°.

Downloaded from https://www.cambridge.org/core. 23 Nov 2024 at 01:21:51, subject to the Cambridge Core terms of use.

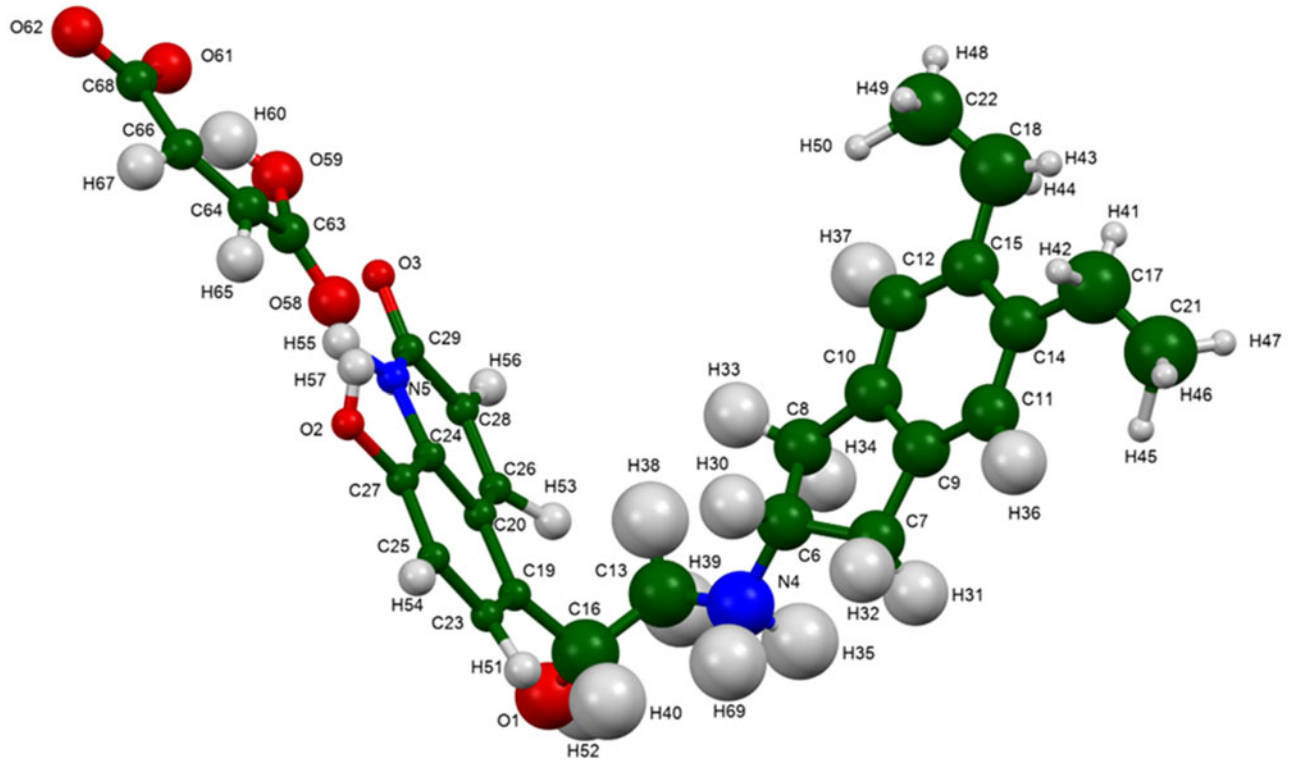

Figure 3. The asymmetric unit of indacaterol hydrogen maleate, with the atom numbering. The atoms are represented by 50% probability spheroids/ellipsoids. Image generated using Mercury (Macrae et al., 2020).

the H, C, N, and O atoms in the calculation were those of Gatti et al. (1994). The calculations were run on a 3.5-GHz PC using 8 *k*-points and the B3LYP functional, and took ~3.9 h.

III. RESULTS AND DISCUSSION

The asymmetric unit contains one indacaterol cation and one hydrogen maleate anion (Figure 3). The compound is thus correctly described as indacaterol hydrogen maleate. The root-mean-square (rms) Cartesian displacement of the non-H atoms in the Rietveld-refined and VASP-optimized cation structures is 0.232 Å (Figure 4); the equivalent quantity for the anions is 0.221 Å. The agreement is within the normal range for correct structures (van de Streek and Neumann, 2014), and provides confirmation that the structure is correct. The remainder of this discussion will emphasize the VASP-optimized structure.

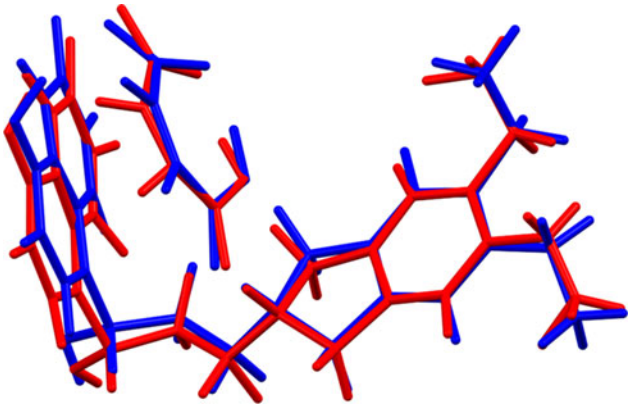

Figure 4. Comparison of the Rietveld-refined (red) and VASP-optimized (blue) structures of indacaterol hydrogen maleate. The rms Cartesian displacement for the cation is 0.232 Å, and for the anion is 0.221 Å. Image generated using Mercury (Macrae et al., 2020).

The *P*1 structure of YIBRAG and the *P*-1 structure determined here are essentially identical (Figure 5). When applied to YIBRAG, checkCIF (PLATON) yields a Level G alert, indicating the presence of center of symmetry, with a 97% fit. The centrosymmetric model is more chemically-reasonable, especially when fitting powder (even synchrotron) data, even though the *P*1 model yields lower residuals (more variables) and highly-correlated parameters. A positive second harmonic generation test could establish the absence of a center of symmetry.

Almost all of the bond distances and bond angles fall within the normal ranges indicated by a Mercury Mogul Geometry check (Macrae et al., 2020). Only the C13–C16–C19 angle of 115.5° (average = 109.1(20)°, *Z*-score = 3.2) is flagged as unusual. The torsion angles involving rotation about the C3–N4, C13–C16, and C16–C19 bonds are flagged as unusual. They lie on the tails of broad distributions, and reflect the orientation of the two parts of the cation, and the protonation at N4. The conformation of the cation is unusual.

Quantum chemical geometry optimization of the isolated cation (DFT/B3LYP/6-31G*/water) using Spartan '20 (Wavefunction, 2022) indicated that the solid-state conformation of the cation is 9.3 kcal/mol higher in energy than the local minimum, which is similar but has a different orientation of the quinoline ring system with respect to the rest of the cation. The global minimum-energy conformation of the cation is considerably more compact, with parallel ring systems. The

Downloaded from https://www.cambridge.org/core. 23 Nov 2024 at 01:21:51, subject to the Cambridge Core terms of use.

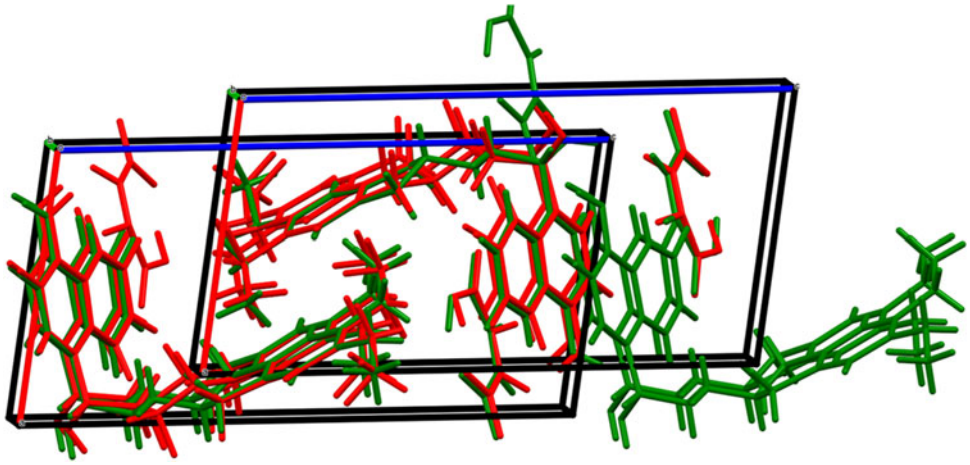

Figure 5. Comparison of the *P*-1 structure of indacaterol hydrogen maleate determined here (red) to the *P*-1 structure of YIBRAG (green). Image generated using Mercury (Macrae et al., 2020).

solid-state conformation of the anion is 3.0 kcal/mol higher in energy than the local minimum, which is planar. The differences show that intermolecular interactions are important in determining the solid-state conformations.

The crystal structure (Figure 6) consists of layers of cations and anions parallel to the *ab*-plane. Traditional N–H···O and O–H···O hydrogen bonds link the cations and anions into chains along the *a*-axis (Figure 7). The mean plane of the quinoline ring system is approximately 1,6,−20, and that of the indene ring system is 7,3,7. The mean plane of the anion is approximately 3,6,−14, but it is significantly non-planar; the O61–C68–C66–C64 torsion angle is −34.0°, and the O59–C63–C64–C66 torsion is 20.5°. The Mercury Aromatic Analyser indicates only weak interactions, with the strongest between quinoline rings at a distance of 4.4 Å.

Analysis of the contributions to the total crystal energy of the structure using the Forcite module of Materials Studio

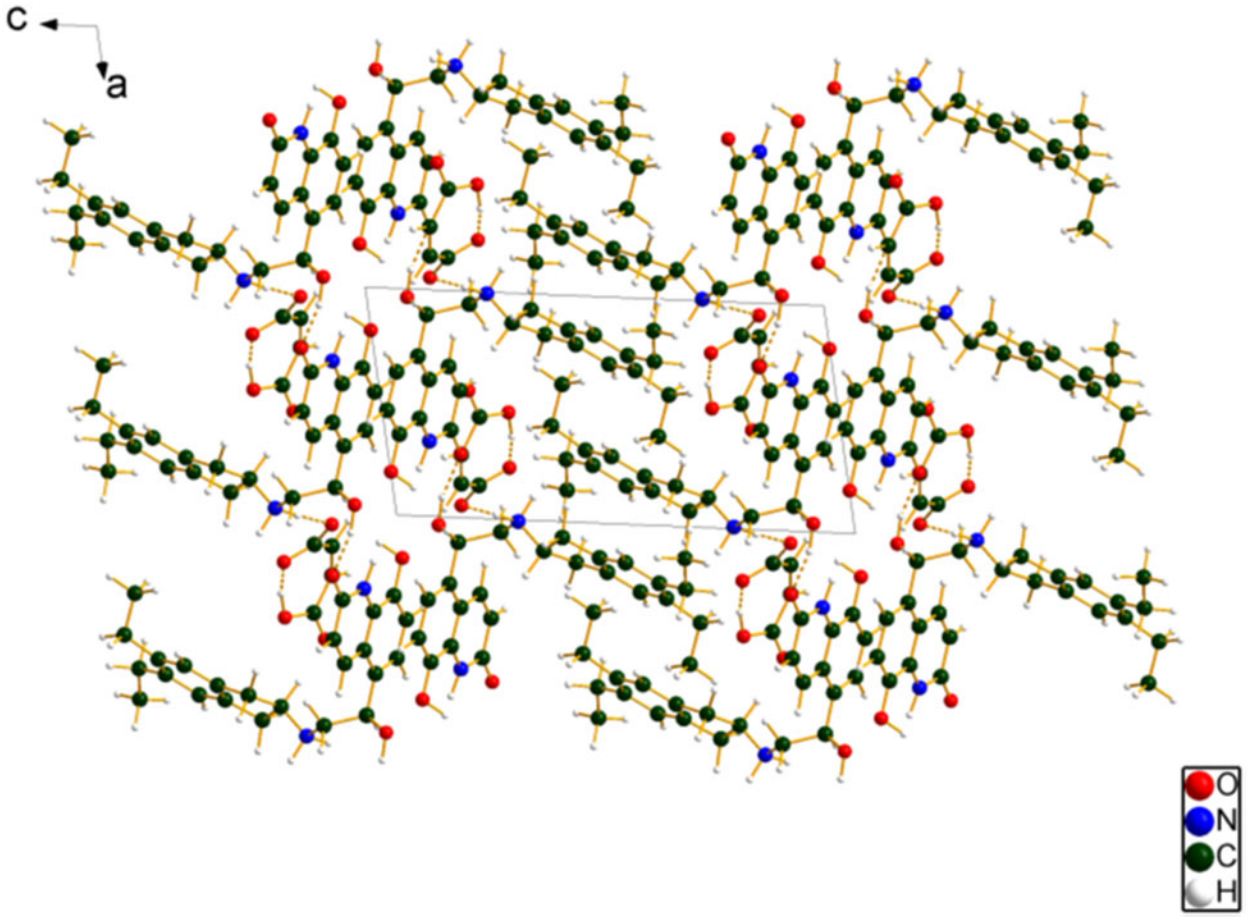

Figure 6. The crystal structure of indacaterol hydrogen maleate, viewed down the *b*-axis. Image generated using Diamond (Crystal Impact, 2023).

Downloaded from https://www.cambridge.org/core. 23 Nov 2024 at 01:21:51, subject to the Cambridge Core terms of use.

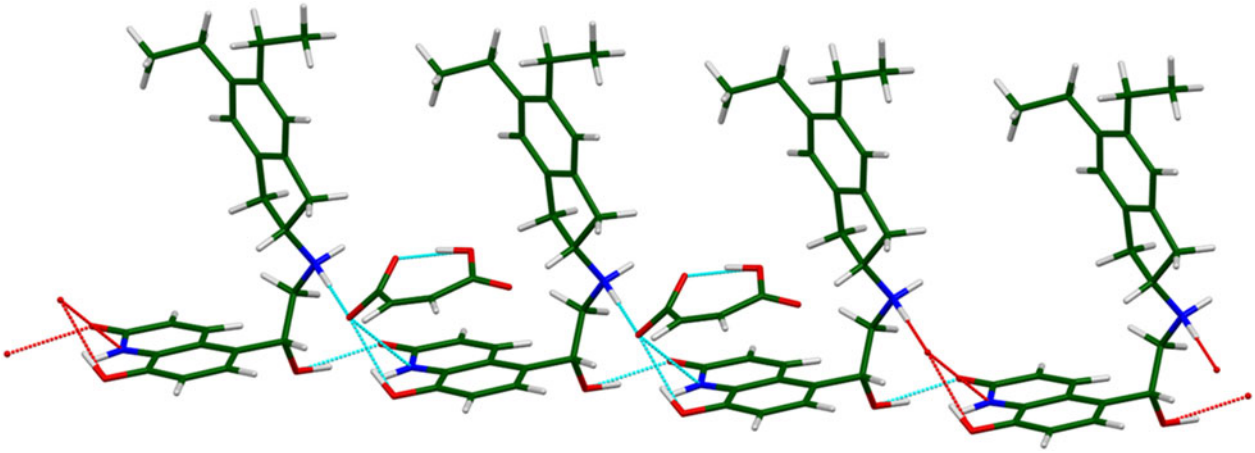

Figure 7. The hydrogen bonded chains along the *a*-axis of cations and anions in indacaterol hydrogen maleate. Image generated using Mercury (Macrae et al., 2020).

TABLE I. Hydrogen bonds (CRYSTAL23) in indacaterol hydrogen maleate.

H-bond	D–H, Å	H···A, Å	D···A, Å	D–H···A,°	Overlap, *e*	*E*, kcal/mol
O59–H60···O61	1.027	1.424[a]	2.486	168.7	0.095	16.8
C66–H67···O2	1.081	2.284	3.388	168.6	0.025	
C64–H65···O3	1.089	2.188	3.028	132.0	0.017	
N4–H69···O62	1.068	1.705	2.779	177.9	0.088	6.8
N4–H35···C15	1.018	2.549	3.563	162.2	0.015	
O1–H52···O3	0.976	1.680	2.687	163.9	0.058	13.2
N5–H55···O2	1.003	2.424[a]	2.795	100.4	0.016	2.9
N5–H55···O1	1.003	2.732	2.746	137.1	0.014	2.7
C6–H30···O58	1.084	2.130	3.185	157.3	0.035	
C18–H44···O61	1.105	2.487	3.586	172.6	0.020	
C28–H56···O58	1.090	2.347	3.240	137.6	0.020	
C26–H53···O1	1.068	2.481	2.507	112.5	0.017	
C21–H47···O61	1.098	2.658	3.721	163.0	0.013	
C25–H54···O58	1.090	2.808	2.810	132.2	0.011	
C8–H33···O59	1.079	2.596	2.615	109.1	0.010	
C16–H40···O62	1.097	2.357	3.352	146.9	0.010	

[a]Intramolecular.

(Dassault Systèmes, 2022) suggests that bond, angle, and torsion distortion terms contribute about equally to the intramolecular energy. The intermolecular energy is dominated by electrostatic attractions, which in this force field analysis include hydrogen bonds. The hydrogen bonds are better analyzed using the results of the density functional theory (DFT) calculation.

As expected, there is a strong intramolecular charge-assisted O–H···O hydrogen bond in the hydrogen maleate anion (Table I). There are also two C–H···O hydrogen bonds between the anion and cation. The cation makes a strong N4–H69···O62 hydrogen bond to the anion, but N4–H35 acts as a hydrogen bond donor to the aromatic C15. The amino group N5–H55 makes bifurcated N–H···O hydrogen bonds, one intramolecular to O2 and the other intermolecular to O1 in another cation. The hydroxyl group O1–H52 acts as a donor to O3 in another cation. Several C–H···O hydrogen bonds link cations and anions, as well as cations to other cations.

The volume enclosed by the Hirshfeld surface of indacaterol hydrogen maleate (Figure 8, Hirshfeld, 1977; Spackman et al., 2021) is 626.48 Å^3, 98.41% of the unit cell volume. The packing density is thus fairly typical. The only significant

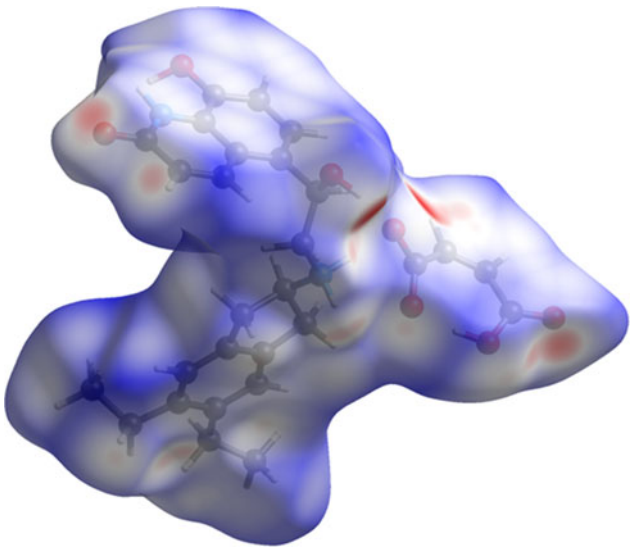

Figure 8. The Hirshfeld surface of indacaterol hydrogen maleate. Intermolecular contacts longer than the sums of the van der Waals radii are colored blue, and contacts shorter than the sums of the radii are colored red. Contacts equal to the sums of radii are white. Image generated using CrystalExplorer (Spackman et al., 2021).

Downloaded from https://www.cambridge.org/core. 23 Nov 2024 at 01:21:51, subject to the Cambridge Core terms of use.

close contacts (red in Figure 8) involve the hydrogen bonds. The volume/non-hydrogen atom is smaller than usual, at 17.2 Å^3, reflecting the strong hydrogen bonds.

The Bravais–Friedel–Donnay–Harker (Bravais, 1866; Friedel, 1907; Donnay and Harker, 1937) morphology suggests that we might expect platy morphology for indacaterol hydrogen maleate, with {001} as the major faces. A second-order spherical harmonic model was included in the refinement. The texture index was 1.006(0), indicating that preferred orientation was not significant in this rotated capillary specimen.

IV. DEPOSITED DATA

The powder pattern of indacaterol maleate from this synchrotron data set has been submitted to ICDD for inclusion in the Powder Diffraction File. The Crystallographic Information Framework (CIF) files containing the results of the Rietveld refinement (including the raw data) and the DFT geometry optimization were deposited with the ICDD. The data can be requested at pdj@icdd.com.

ACKNOWLEDGEMENTS

Use of the Advanced Photon Source at Argonne National Laboratory was supported by the U.S. Department of Energy, Office of Science, Office of Basic Energy Sciences, under Contract No. DE-AC02-06CH11357. This work was partially supported by the International Centre for Diffraction Data. We thank Saul Lapidus for his assistance in the data collection.

CONFLICTS OF INTEREST

The authors have no conflicts of interest to declare.

REFERENCES

Altomare, A., C. Cuocci, C. Giacovazzo, A. Moliterni, R. Rizzi, N. Corriero, and A. Falcicchio. 2013. "EXPO2013: A Kit of Tools for Phasing Crystal Structures from Powder Data." *Journal of Applied Crystallography* 46: 1231–5.

Antao, S. M., I. Hassan, J. Wang, P. L. Lee, and B. H. Toby. 2008. "State-of-the-Art High-Resolution Powder X-ray Diffraction (HRPXRD) Illustrated with Rietveld Refinement of Quartz, Sodalite, Tremolite, and Meionite." *Canadian Mineralogist* 46: 1501–9.

Baur, F., D. Beattie, D. Beer, D. Bentley, M. Bradley, I. Bruce, S. J. Charlton, B. Cuenroud, R. Ernst, R. A. Fairhurst, B. Faller, D. Farr, T. Keller, J. R. Fozard, J. Fullerton, S. Garman, J. Hatto, C. Hayden, H. He, C. Howes, D. Janus, Z. Jiang, C. Lewis, F. Loeuillet-Ritzler, H. Moser, J. Reilly, A. Steward, L. Tedaldi, A. Trifileff, M. Tweed, S. Watson, E. Wissler, and D. Wyss. 2010. "The Identification of Indacaterol as an Ultralong-Acting Inhaled β_2-Adrenoceptor Agonist." *Journal of Medicinal Chemistry* 53: 3675–84.

Bravais, A. 1866. *Etudes Cristallographiques*. Paris, Gauthier Villars.

Bruno, I. J., J. C. Cole, M. Kessler, J. Luo, W. D. S. Motherwell, L. H. Purkis, B. R. Smith, R. Taylor, R. I. Cooper, S. E. Harris, and A. G. Orpen. 2004. "Retrieval of Crystallographically-Derived Molecular Geometry Information." *Journal of Chemical Information and Computer Sciences* 44: 2133–44.

Crystal Impact. 2023. Diamond. V. 5.0.0. Crystal Impact - Dr. H. Putz & Dr. K. Brandenburg. Windows.

Cuffini, S. L., S. Faudone, M. Ferro, M. T. Garland, and R. Baggio. 2008. "Rosiglitazone maleate 0.25-hydrate: a pseudopolymorphic form." *Acta crystallographica section C: crystal structure communications* 64: o119–22. doi:10.1107/S0108270107054443.

Dassault Systèmes. 2022. *Materials Studio 2023*. San Diego, CA, BIOVIA.

Donnay, J. D. H., and D. Harker. 1937. "A New Law of Crystal Morphology Extending the Law of Bravais." *American Mineralogist* 22: 446–47.

Erba, A., J. K. Desmarais, S. Casassa, B. Civalleri, L. Donà, I. J. Bush, B. Searle, L. Maschio, L.-E. Daga, A. Cossard, C. Ribaldone, E. Ascrizzi, N. L. Marana, J.-P. Flament, and B. Kirtman. 2023. "CRYSTAL23: A Program for Computational Solid State Physics and Chemistry." *Journal of Chemical Theory and Computation* 19: 6891–932. doi:10.1021/acs.jctc.2c00958.

Friedel, G. 1907. "Etudes sur la loi de Bravais." *Bulletin de la Société Française de Minéralogie* 30: 326–455.

Gates-Rector, S., and T. N. Blanton. 2019. "The Powder Diffraction File: A Quality Materials Characterization Database." *Powder Diffraction* 39: 352–60.

Gatti, C., V. R. Saunders, and C. Roetti. 1994. "Crystal-Field Effects on the Topological Properties of the Electron-Density in Molecular Crystals - the Case of Urea." *Journal of Chemical Physics* 101: 10686–96.

Groom, C. R., I. J. Bruno, M. P. Lightfoot, and S. C. Ward. 2016. "The Cambridge Structural Database." *Acta Crystallographica Section B: Structural Science, Crystal Engineering and Materials* 72: 171–9.

Hirshfeld, F. L. 1977. "Bonded-Atom Fragments for Describing Molecular Charge Densities." *Theoretica Chemica Acta* 44: 129–38.

Kaduk, J. A., C. E. Crowder, K. Zhong, T. G. Fawcett, and M. R. Suchomel. 2014. "Crystal Structure of Atomoxetine Hydrochloride (Strattera), $C_{17}H_{22}NOCl$." *Powder Diffraction* 29: 269–73.

Kim, S., J. Chen, T. Cheng, A. Gindulyte, J. He, S. He, Q. Li, B. A. Shoemaker, P. A. Thiessen, B. Yu, L. Zaslavsky, J. Zhang, and E. E. Bolton. 2023. "Pubchem 2023 update." *Nucleic Acids Research* 51 (D1): D1373–80. doi:10.1093/nar/gkac956.

Kresse, G., and J. Furthmüller. 1996. "Efficiency of Ab-Initio Total Energy Calculations for Metals and Semiconductors Using a Plane-Wave Basis Set." *Computational Materials Science* 6: 15–50.

Lee, P. L., D. Shu, M. Ramanathan, C. Preissner, J. Wang, M. A. Beno, R. B. Von Dreele, L. Ribaud, C. Kurtz, S. M. Antao, X. Jiao, and B. H. Toby. 2008. "A Twelve-Analyzer Detector System for High-Resolution Powder Diffraction." *Journal of Synchrotron Radiation* 15: 427–32.

Macrae, C. F., I. Sovago, S. J. Cottrell, P. T. A. Galek, P. McCabe, E. Pidcock, M. Platings, G. P. Shields, J. S. Stevens, M. Towler, and P. A. Wood. 2020. "Mercury 4.0: From Visualization to Design and Prediction." *Journal of Applied Crystallography* 53: 226–35.

Materials Design. 2016. *MedeA 2.20.4*. Angel Fire, NM, Materials Design Inc.

McGrath, N. A., M. Brichacek, and J. T. Njardarson. 2010. "A Graphical Journey of Innovative Organic Architectures That Have Improved Our Lives." *Journal of Chemical Education* 87 (12): 1348–49. doi:10.1021/ed1003806.

Spackman, P. R., M. J. Turner, J. J. McKinnon, S. K. Wolff, D. J. Grimwood, D. Jayatilaka, and M. A. Spackman. 2021. "Crystalexplorer: A Program for Hirshfeld Surface Analysis, Visualization and Quantitative Analysis of Molecular Crystals." *Journal of Applied Crystallography* 54: 1006–11. doi:10.1107/S1600576721002910.

Spek, A. L. 2009. "Structure Validation in Chemical Crystallography." *Acta Crystallographica D* 65: 148–55.

Spek, A. L. 2020. "CheckCIF Validation Alerts: What They Mean and How To Respond." *Acta Crystallographica E* 76: 1–11.

Sykes, R. A., P. McCabe, F. H. Allen, G. M. Battle, I. J. Bruno, and P. A. Wood. 2011. "New Software for Statistical Analysis of Cambridge Structural Database Data." *Journal of Applied Crystallography* 44: 882–6.

Toby, B. H., and R. B. Von Dreele. 2013. "GSAS II: The Genesis of a Modern Open Source All Purpose Crystallography Software Package." *Journal of Applied Crystallography* 46: 544–9.

van de Streek, J., and M. A. Neumann. 2014. "Validation of Molecular Crystal Structures from Powder Diffraction Data with Dispersion-Corrected Density Functional Theory (DFT-D)." *Acta Crystallographica Section B: Structural Science, Crystal Engineering and Materials* 70: 1020–32.

Wang, J., B. H. Toby, P. L. Lee, L. Ribaud, S. M. Antao, C. Kurtz, M. Ramanathan, R. B. Von Dreele, and M. A. Beno. 2008. "A Dedicated Powder Diffraction Beamline at the Advanced Photon Source: Commissioning and Early Operational Results." *Review of Scientific Instruments* 79: 085105.

Wavefunction, Inc. 2022. *Spartan '20. V. 1.1.4*. Irvine, CA: Wavefunction Inc.

Downloaded from https://www.cambridge.org/core. 23 Nov 2024 at 01:21:51, subject to the Cambridge Core terms of use.